



Contents lists available at ScienceDirect

Thin Solid Films

journal homepage: www.elsevier.com/locate/tsf

Electrical conduction through self-assembled monolayers in molecular junctions: Au/molecules/Au versus Au/molecule/PEDOT:PSS/Au

Gunuk Wang, Hana Yoo, Seok-In Na, Tae-Wook Kim, Byungjin Cho, Dong-Yu Kim, Takhee Lee *

Department of Materials Science and Engineering, Gwangju Institute of Science and Technology, Gwangju 500-712, Republic of Korea

ARTICLE INFO

Available online 12 July 2009

Keywords:

Self-assembled monolayer
Molecular junction
Octanedithiol
Transport mechanism

ABSTRACT

We fabricated and characterized a large number of octanedithiol (denoted as DC8) molecular devices as vertical metal–molecule–metal structure with or without using an intermediate conducting polymer layer of poly(3,4-ethylenedioxythiophene) stabilized with poly(4-styrenesulfonic acid) (called as PEDOT:PSS). The electronic transport properties of DC8 molecular devices with and without PEDOT:PSS layer were statistically compared in terms of current density and device yield. The yields of the working molecular devices were found to be ~1.75% (84 out of 4800 devices) for Au/DC8/Au junctions and ~58% (74 out of 128 devices) for Au–DC8/PEDOT:PSS/Au junctions. The tunneling decay constants were obtained with the Simmons tunneling model and a multibarrier tunneling model for two kinds of molecular devices with and without PEDOT:PSS layer.

© 2009 Elsevier B.V. All rights reserved.

1. Introduction

Electronic transport through molecular layers has been extensively studied with a variety of device geometries for understanding the conduction mechanism and realizing potential device applications [1–6]. The alkanethiol self-assembled monolayers (SAMs) sandwiched between Au electrodes has been one of the most popular molecular systems for study due to the robust formation of monolayers of alkanethiol SAMs on Au surface and simple device processing [3,7–12]. However, the electrical shorts in metal–molecule–metal (M–M–M) junction devices often occurred due to the penetration by top electrode metals through thin molecular layer, which leads to the limitation of working device yield [9]. For example, the working device yield of alkanethiol molecular devices in the microscale (diameter of ~2 μm) M–M–M junction was reported to be ~1–2% [9]. The device yield improved a little bit up to ~7% when the alkanethiol molecular devices were fabricated in the nanoscale (diameter of ~50 nm) M–M–M junctions [10]. A recent study, with the objective of preventing electrical shorts by using a layer of a highly conducting polymer (poly(3,4-ethylenedioxythiophene) stabilized with poly(4-styrenesulfonic acid)) (called as PEDOT:PSS) resulted in a remarkable improvement in the yield (~95%) of molecular electronic devices even in the very large junction size (diameter of ~100 μm) [11]. In spite of this very high device yield, the molecular junctions with PEDOT:PSS layer would be different from the molecular junctions without PEDOT:PSS layer due to the different contact properties [12]. Therefore, a comprehensive analysis of difference of the electronic conduction between both types of device

structures i.e., molecular junctions with and without PEDOT:PSS layer would be thoroughly established.

In this study, we characterized a large number of octanedithiol (HS(CH₂)₈SH; denoted as DC8) molecular electronic devices fabricated in two structures with and without using PEDOT:PSS intermediate layer in vertical M–M–M junctions. The average transport parameters such as current densities and decay constants in two types of molecular device structures were obtained from the statistically defined working molecular devices with the Simmons tunneling model and a multibarrier tunneling model.

2. Experimental details

2.1. Device fabrication

DC8 molecular electronic devices were fabricated in two types of structures, as schematically illustrated in Fig. 1. As shown in Fig. 1(a), Au/DC8/Au molecular devices were fabricated as vertical M–M–M structures with microscale via-hole junctions (circular shape with diameter of ~2 μm) where molecular monolayers were sandwiched between the top and bottom Au electrodes. On the contrary, Au/DC8/PEDOT:PSS/Au molecular devices (Fig. 1(b)) were fabricated with a large device area (square shape with side length of 30 to 100 μm) with the conducting polymer PEDOT:PSS as intermediate top electrode. Images of fabricated devices have been reported previously elsewhere [9]. First, a conventional optical lithography method was used to pattern the bottom electrodes made with Au (1000 Å)/Ti (50 Å) on a p-type (100) Si substrate covered with thermally grown 3000 Å thick SiO₂ by an electron beam evaporator under a pressure of ~10⁻⁷ Torr. Then, a SiO₂ layer (700 Å thick) was deposited using plasma enhanced

* Corresponding author. Tel.: +82 62 970 2313; fax: +82 62 970 2304.
E-mail address: tlee@gist.ac.kr (T. Lee).

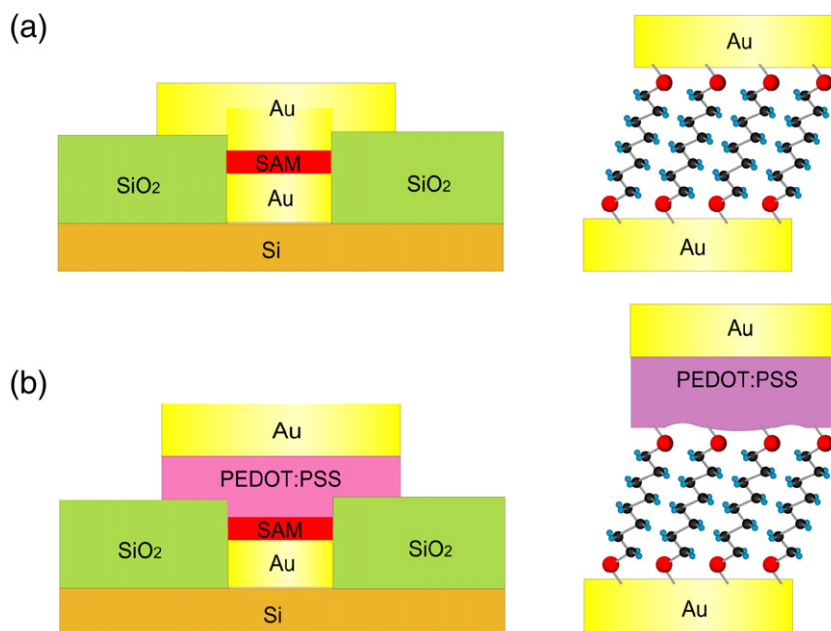


Fig. 1. Schematics of micro-via hole molecular device structures (a) without PEDOT:PSS and (b) with PEDOT:PSS. The configurations of Au/DC8/Au and Au/DC8/PEDOT:PSS/Au junctions are shown in the right side.

chemical vapor deposition (PECVD). In case of Au/DC8/Au devices, reactive ion etching (RIE) was performed to make a circular via-hole with 2 μm in diameter through the SiO_2 layer to expose the bottom Au electrode surface. The DC8 SAMs were formed on the exposed Au surfaces, and top Au electrode was formed to complete the molecular junction by a thermal evaporator. The evaporation for top electrodes was done with a shadow mask on the chips, with a liquid nitrogen cooled cold stage to avoid thermal damage to the active molecular component, under a pressure of $\sim 10^{-6}$ Torr. For the same reason, the deposition rate of the top Au electrode was kept very low, typically at ~ 0.1 $\text{\AA}/\text{s}$ to form a total Au thickness of ~ 500 \AA .

In case of Au/DC8/PEDOT:PSS/Au devices, buffered oxide etching (BOE) was performed for 1 min to make square via-holes with side length of 30 to 100 μm through SiO_2 layer. After DC8 SAMs were formed on the exposed bottom Au electrode, a water based suspension conducting polymer PEDOT:PSS was spin coated with two steps (first step at 500 rpm for 5 s, second step at 3000 rpm for 35 s) over the chips in a nitrogen-filled glove box with oxygen of less than ~ 10 ppm. The thickness of PEDOT:PSS was ~ 100 nm measured by a surface profiler (Kosaka ET-3000i). PEDOT:PSS used in our study is a commercially available (from H. C. Starck) and highly doped polymer with a conductivity of about 300 S cm^{-1} [13]. Then, the top Au electrode was deposited on top of the PEDOT:PSS layer using an electron beam evaporator through a shadow mask. RIE with O_2 was used to remove the redundant PEDOT:PSS. The Au top electrode was used as a good contact with the probes and as a shadow mask while PEDOT:PSS was etched away using RIE to prevent direct current path through PEDOT:PSS from top to bottom electrode. The current-voltage (I - V) characteristics of the fabricated molecular devices were carried out using semiconductor parameter analyzers (HP4155A and Keithley 4200-SCS) at room temperature.

2.2. Formation of self-assembled monolayers

For our experiments, ~ 5 mM octanedithiol ($\text{HS}(\text{CH}_2)_8\text{SH}$, DC8) solutions were prepared by adding ~ 10 μL DC8 to ~ 10 mL anhydrous ethanol (Aldrich Chem. Co). The samples were left in the solution for 24–48 h to allow DC8 SAMs to form on the Au surfaces exposed by RIE in a nitrogen-filled glove box. DC8 SAMs were used to form the active molecular components in molecular devices. As an example, the

configurations of Au/DC8/Au and Au/DC8/PEDOT:PSS/Au junctions are shown in Fig. 1.

3. Results and discussion

3.1. Tunneling current densities of Au/DC8/Au and Au/DC8/PEDOT:PSS/Au devices

For this study, we fabricated statistically sufficient number of molecular devices with different top contacts (with and without PEDOT:PSS layer) and characterized their electronic properties. The “working” molecular devices were determined based on the statistical distribution of the current densities of the fabricated devices. Basically, working molecular electronic devices were extracted from devices showing a majority of current densities in the statistical distribution, by using Gaussian function, as shown in Fig. 2(a). The detailed criterion for determining working devices has been reported elsewhere [9]. As summarized in Table 1, the numbers of Au/DC8/Au and Au/DC8/PEDOT:PSS/Au working devices were determined as 84 out of fabricated 4800 devices and 74 out of fabricated 128 devices, respectively. Therefore, the device yields are $\sim 1.75\%$ (84/4800) for Au/DC8/Au devices and $\sim 58\%$ (74/128) for Au/DC8/PEDOT:PSS/Au devices. In case of Au/DC8/Au devices, the device yield is very low due to the electrical shorts caused by the penetration of Au top electrode through the thin molecular layer [9]. On the other hand, in case of Au/DC8/PEDOT:PSS/Au devices, interlayer of the higher conducting polymer PEDOT:PSS between molecular SAM and Au top electrode effectively prevent electrical shorts by top Au electrode penetration, which results in a remarkable improvement in the yield of molecular devices [11].

In addition to the device yield, detail transport parameters are also different between these two types of molecular devices (Au/DC8/Au versus Au/DC8/PEDOT:PSS/Au). Fig. 2(a) presents statistical histograms of current densities (J) in logarithmic scale for Au/DC8/Au and Au/DC8/PEDOT:PSS/Au at 1.0 V with the mean positions indicated with arrows from the fitting results by Gaussian functions. The devices at the mean positions can be considered as the “representative devices” [9]. The logarithmic values of the average current densities for the all working devices were found to be 5.5 ± 0.28 and 2.48 ± 0.19 at 1.0 V for Au/DC8/Au and Au/DC8/PEDOT:PSS/Au junctions,

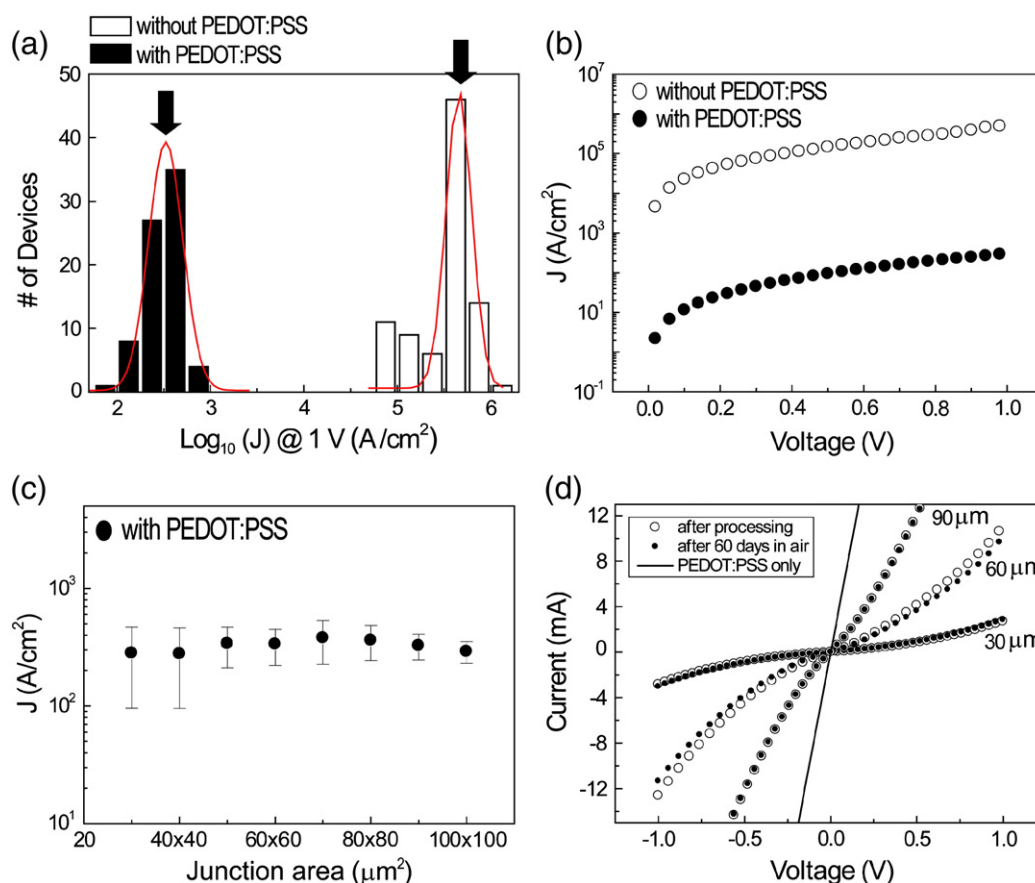


Fig. 2. (a) The statistical histograms of $\log J$ measured at 1.0 V for Au/DC8/Au and Au/DC8/PEDOT:PSS/Au junctions. The line curves are fitting results obtained with Gaussian functions and the mean positions are indicated with black arrows. (b) J - V characteristics of representative devices chosen from the mean positions of the fitted Gaussian functions. (c) The current density measured at 1.0 V for Au/DC8/PEDOT:PSS/Au junctions with different junction areas. (d) I - V characteristics of Au/DC8/PEDOT:PSS/Au junctions with side lengths of 30, 60, and 90 μm , measured immediately after fabrication and after storage under ambient condition for 60 days. The solid line was observed for a PEDOT:PSS only device (side length of 30 μm) without DC8 SAM, indicating ohmic curve.

respectively. Note that the distribution of logarithmic current densities (Fig. 2(a)) are attributed to some fluctuations in molecular configurations in the SAMs in the junctions such as molecular tilting angle, surface flatness of the Au bottom electrode, and microstructures in contacts [9,14–16].

The characteristics of the representative devices are plotted in Fig. 2(b). The current density for Au/DC8/Au was observed about 3 orders of magnitude higher than that for Au/DC8/PEDOT:PSS/Au device, which is due to the different nature of contact properties. Au/DC8/Au device has chemisorbed contacts [Au–S–C] on the both sides of the molecules (Fig. 1(a)), whereas Au/DC8/PEDOT:PSS/Au device has only one chemisorbed contact [Au–S–C] at one side and a physisorbed contact [C–SH/PEDOT:PSS] at the other side (Fig. 1(b)) [12]. Note that the chemisorbed contacts in molecular junction is known to have less contact resistance due to formation strong bondings by molecular overlapping, thus charge transport is more efficient through chemisorbed contacts than the physisorbed contacts [15]. Furthermore, the nature of physisorbed contact for the DC8/PEDOT:PSS interface is not well established. The morphology of spin-cast PEDOT:PSS film is like pancake-shaped PEDOT-rich islands with a

thickness of a few nanometer and a diameter of a few tens of nanometers separated by quasi continuous non-conducting PSS lamellas [17]. Therefore, the charge conduction through PEDOT:PSS layer takes place mainly in PEDOT-rich domains via hopping of charge carrier [17,18]. Although it is difficult to know the exact contact morphology and microstructure in DC8/PEDOT:PSS interface, the main conduction path presumably occurs through the DC8/PEDOT interface region than DC8/PSS region. The conduction disparity at the contact interfaces (DC8/PEDOT vs DC8:PSS) results in the reduction of the conduction area of DC8/PEDOT:PSS interface region. In this sense, the reduction of current density in Au/DC8/PEDOT:PSS/Au devices compared with that in Au/DC8/Au devices can be explained by the physisorbed contact of DC8/PEDOT interface and the reduction of conduction area.

Fig. 2(c) shows current densities as a function of the side length (30 to 100 μm) of the square junctions for Au/DC8/PEDOT:PSS/Au devices. This graph shows area-independent current densities for Au/DC8/PEDOT:PSS/Au devices, suggesting that the variation of morphology of DC8/PEDOT:PSS interface is negligible as variation of the junction area. Fig. 2(d) shows the I - V characteristics of Au/DC8/

Table 1
Summary of results for the fabricated devices.

	# of fabricated devices	Fab. failure	Short	Open	Non-working	Working
DC8	4800 (100%)	192 (4%)	4080 (85%)	428 (8.9%)	16 (0.3%)	84 (1.75%)
DC8/PEDOT:PSS	128 (100%)	4 (3%)	35 (27%)	0 (0%)	15 (12%)	74 (58%)

PEDOT:PSS/Au junctions with side lengths of 30, 60, and 90 μm , measured immediately after fabrication and after storage under ambient condition for 60 days. This result shows stable and reproducible charge transport properties through DC8/PEDOT:PSS layers. In contrast, the I - V characteristics for Au/DC8/Au devices sometimes degraded after a few days, which may be due to the reorganization of top contact sites (DC8/Au) or reformation short paths between top and bottom electrodes. The linear I - V ohmic feature in Fig. 2(d) was observed for the PEDOT:PSS only devices with a higher current than that for devices containing DC8 SAM.

3.2. Tunneling model

We investigated the difference of conduction properties between Au/DC8/Au and Au/DC8/PEDOT:PSS/Au devices with the Simmons tunneling model [19] which is a widely used model for describing a rectangular tunneling barrier and has been used to explain the tunneling transport through SAM junctions. Simmons tunneling model is expressed as Eq. (1),

$$J = \left(\frac{e}{4\pi^2 \hbar d^2} \right) \left\{ \left(\Phi_B - \frac{eV}{2} \right) \exp \left[-\frac{2(2m)^{1/2}}{\hbar} \alpha \left(\Phi_B - \frac{eV}{2} \right)^{1/2} d \right] - \left(\Phi_B + \frac{eV}{2} \right) \exp \left[-\frac{2(2m)^{1/2}}{\hbar} \alpha \left(\Phi_B + \frac{eV}{2} \right)^{1/2} d \right] \right\} \quad (1)$$

where m is the electron mass, d is the barrier width, Φ_B is the barrier height, V is the applied bias, and α is a unit less adjustable parameter that can be used to differentiate between potential barrier shapes, or to describe the effective mass of electron. In the low bias regime (or ohmic region), the current density can be approximated as,

$$J \approx \frac{(2m\Phi_B)^{1/2} e^2 \alpha}{4\pi^2 \hbar^2 d} V \exp[-\beta_0 d], \quad (2)$$

$$\beta_0 = \frac{2(2m)^{1/2}}{\hbar} \alpha (\Phi_B)^{1/2}$$

where β_0 is the overall decay constant in the low bias regime, which reflects the degree of decrease in wavefunction of the tunneling electron through the overall molecular tunnel barrier. Although the transport fitting parameters from the Simmons model does not give the precise information for the charge transport accurately, this model can give some rough idea of the charge transport and conductance magnitudes in the experimental point of view.

We performed the Simmons tunneling fitting (using Eq. (1)) on all the working devices of Au/DC8/Au and Au/DC8/PEDOT:PSS/Au junctions to statistically obtain the overall decay constant β_0 values. In the calculation, we didn't consider the thickness of PEDOT:PSS layer into the barrier width d , because electron tunneling occurs only in molecular layer [12,15]. Fig. 3 shows the distribution of β_0 values of all of the individual working Au/DC8/Au (~84 devices) and Au/DC8/PEDOT:PSS/Au (~74 devices) devices from the Simmons tunneling fittings. The statistical mean β_0 values were found to be $0.55 \pm 0.06 \text{ \AA}^{-1}$ and $1.06 \pm 0.04 \text{ \AA}^{-1}$ for Au/DC8/Au and Au/DC8/PEDOT:PSS/Au devices, respectively. A higher decay constant implies a faster decay of the wavefunction, i.e., lower electron tunneling efficiency. This result suggests that the electron transmission for Au/DC8/Au is found to be more efficient than that for the Au/DC8/PEDOT:PSS/Au due to the difference natures of the contact properties (C-S-Au versus C-SH/PEDOT:PSS), which is consistent with results of different current densities for these two types of molecular devices (Fig. 2(a),(b)).

To investigate the effect of the different contact properties on the electronic transport in Au/DC8/Au and Au/DC8/PEDOT:PSS/Au devices, we used our previously proposed multibarrier tunneling

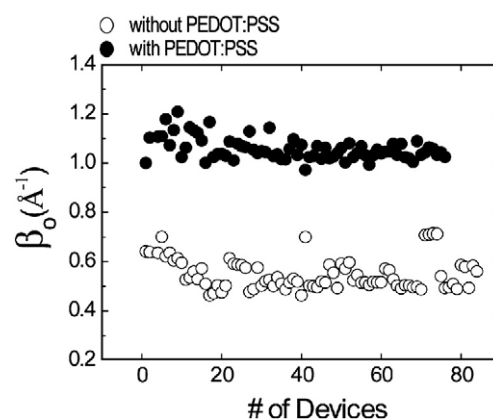


Fig. 3. Statistical distribution of the overall decay constant β_0 values for Au/DC8/Au and Au/DC8/PEDOT:PSS/Au junctions.

(MBT) model [15,20]. In MBT model, the tunneling in the molecular junctions can be divided into three conduction barriers: a molecular body barrier and two contact barriers on either side of molecule. This approach of separating the contacts and molecular body region in a molecular junction is valid when nonresonant tunneling is the main conduction mechanism of the electronic charge transport particularly at a relatively low bias regime. These conditions are well satisfied for the alkanethiol molecular junctions because the Fermi level of the electrodes falls within the relatively large highest occupied molecular orbital (HOMO)-lowest unoccupied molecular orbital (LUMO) gap of the alkanethiol molecules ($\sim 8 \text{ eV}$) [3]. In the MBT model, the magnitude of the β_0 values at the low bias regime describes the overall slope of wavefunction decay through the three individual barriers describe, as illustrated in Fig. 4. And this β_0 value can be decomposed to three individual decays corresponding to the chemisorbed contact barrier, the molecular body barrier, and the physisorbed contact barrier as molecular junction structure. From consideration of geometric configurations (Fig. 4(a),(b)), the overall decay constant β_0 can be expressed as Eq. 3 for Au/DC8/Au and Au/DC8/PEDOT:PSS/Au junctions,

$$\beta_0 = \frac{\beta_C d_1 + \beta_{\text{Body}} d_{\text{Body}} + \beta_{\text{C(P)}} d_{1(2)}}{d_1 + d_{\text{Body}} + d_{1(2)}} \quad (3)$$

where $\beta_{\text{C(P)}}$ is the chemisorbed (physisorbed) contact decay constant corresponding to the chemisorbed (physisorbed) contact width d_1 (d_2), β_{Body} is the decay constant component for the molecular body width d_{Body} . Thus, one should note that the β_{Body} value is the contact independent decay constant that is only dependent on the molecular structure, whereas the β_0 value depends not only on the molecular structures but also on the nature of the contacts. As shown in Fig. 4, the slope of the dotted line for Au/DC8/PEDOT:PSS/Au junction (Fig. 4 (b)) is steeper than that for Au/DC8/Au junction (Fig. 4(a)), indicating the β_0 value of Au/DC8/PEDOT:PSS/Au is larger than that of Au/DC8/Au junction. This is consistent with the obtained Simmons fitting β_0 values (Fig. 3).

In the previously reported results [20], β_C was $\sim 0.05 \text{ \AA}^{-1}$ corresponding to the d_1 ($\sim 3.2 \text{ \AA}$, [C-S-Au]) and β_{Body} was $\sim 0.92 \text{ \AA}^{-1}$ corresponding to the d_{Body} ($\sim 8.75 \text{ \AA}$, [(CH₂)₈]). Note that we assumed d_2 [C-SH/PEDOT:PSS] was $\sim 2.5 \text{ \AA}$, which was obtained from the sum of 1.5 \AA ([C-S]) and 1 \AA (van der Waals radius of hydrogen) [20]. We did not consider a tunneling barrier width inside PEDOT:PSS because transport (tunneling) occurs mainly inside the molecular layer and contact between molecules and PEDOT:PSS layer. Note that we did not observe any difference of current levels between Au/PEDOT:PSS/Au and Au/Au devices.

Then, using Eq. (3) with above values, β_P for [C-SH/PEDOT:PSS] corresponding to d_2 was found as $\sim 2.84 \text{ \AA}^{-1}$ for physisorbed decay

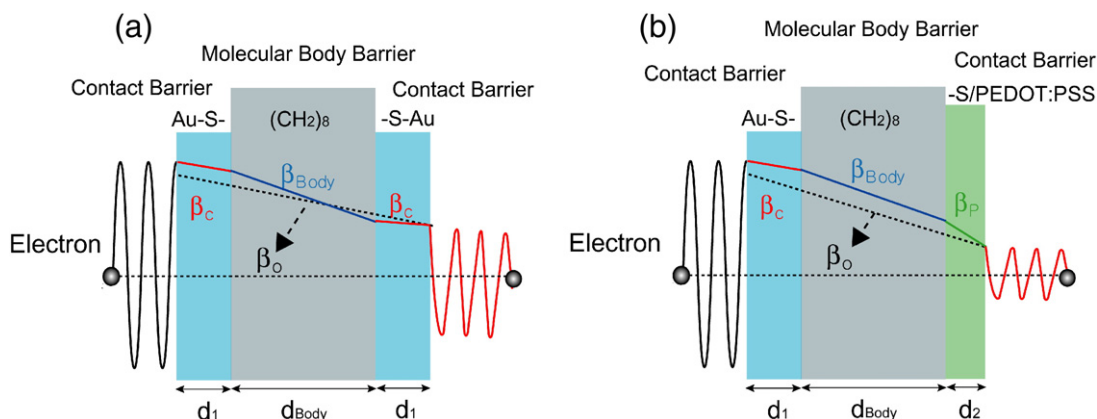


Fig. 4. Schematics of the multibarrier tunneling (MBT) model (a) for Au/DC8/Au (b) for Au/DC8/PEDOT:PSS/Au junctions.

constant. Note this β_p value of DC8/PEDOT:PSS interface is an average effect with various contact structures (DC8/conducting PEDOT-rich domain and DC8/non-conducting PSS). This β_p value of DC8/PEDOT:PSS is higher than the β_p value ($\sim 1.89 \text{ \AA}^{-1}$) for physisorbed contacts [$-\text{CH}_3/\text{Au}$] of a widely studied molecular junction of Au/alkanemonthiol/Au [20], which means lower electron tunneling efficiency at the DC8/PEDOT:PSS interface due to the poor physisorbed contact.

4. Conclusion

We performed a statistical analysis on the electronic transport properties of large number of octanedithiol (DC8) molecular electronic devices with and without using intermediate conducting polymer of PEDOT:PSS layer. From comparison of the charge transport properties of Au/DC8/Au and Au/DC8/PEDOT:PSS/Au junctions, we found that the device yield is much larger, current density is smaller, the overall tunneling decay constant (β_o) is larger for Au/DC8/PEDOT:PSS/Au junctions than the case of Au/DC8/Au junctions.

Acknowledgments

This work was supported by the National Research Laboratory (NRL) Program and the Program for Integrated Molecular System at GIST.

References

- [1] X.D. Cui, A. Primak, X. Zarate, J. Tomfohr, O.F. Sankey, A.L. Moore, T.A. Moore, D. Gust, G. Harris, S.M. Lindsay, *Science* 294 (2001) 571.
- [2] J. Reichert, R. Ochs, D. Beckmann, H.B. Weber, M. Mayor, H. v. Löhneysen, *Phys. Rev. Lett.* 88 (2002) 176804.
- [3] W. Wang, T. Lee, M.A. Reed, *Phys. Rev. B* 68 (2003) 035416.
- [4] A. Szuchmacher Blum, J.G. Kushmerick, D.P. Long, C.H. Patterson, J.C. Yang, J.C. Henderson, Y. Yao, J.M. Tour, R. Shashidha, B.R. Ratna, *Nature Mater.* 4 (2005) 167.
- [5] L. Venkataraman, J.E. Klare, C. Nuckolls, M.S. Hybertsen, M.L. Steigerwald, *Nature* 442 (2006) 904.
- [6] J.E. Green, J.W. Choi, A. Boukai, Y. Bunimovich, E. Johnston-Halperin, E. Delonno, Y. Luo, B.A. Sheriff, K. Xu, Y.S. Shin, H.-R. Tseng, J.F. Stoddart, J.R. Heath, *Nature* 445 (2007) 414.
- [7] J. Jiang, W. Lu, Y. Luo, *Chem. Phys. Lett.* 400 (2004) 336.
- [8] N. Okabayashi, Y. Konda, T. Komeda, *Phys. Rev. Lett.* 100 (2008) 217801.
- [9] T.-W. Kim, G. Wang, H. Lee, T. Lee, *Nanotechnology* 18 (2007) 315204.
- [10] H. Song, N.-J. Choi, H. Lee, T. Lee, *Appl. Phys. Lett.* 91 (2007) 253116.
- [11] H.B. Akkerman, P.W.M. Blom, D.M. de Leeuw, B. de Boer, *Nature* 441 (2006) 69.
- [12] H.B. Akkerman, B. de Boer, *J. Phys.: Condens. Matter* 20 (2008) 013001.
- [13] S.-I. Na, S.-S. Kim, J. Jo, D.-Y. Kim, *Adv. Mater.* 20 (2008) 4061.
- [14] Y. Hu, Y. Zhu, H. Gao, H. Guo, *Phys. Rev. Lett.* 95 (2005) 156803.
- [15] G. Wang, T.-W. Kim, H. Lee, T. Lee, *Phys. Rev. B* 76 (2007) 205320.
- [16] E. Lörtscher, H.B. Weber, H. Riel, *Phys. Rev. Lett.* 98 (2007) 176807.
- [17] A.M. Nardes, M. Kemerink, R.A.J. Janssen, J.A.M. Bastiaansen, N.M.M. Kiggen, B.M.W. Langeveld, A.J.J.M. van Breemen, M.M. de Kok, *Adv. Mater.* 19 (2007) 1196.
- [18] A.M. Nardes, R.A.J. Janssen, M. Kemerink, *Adv. Funct. Mater.* 18 (2008) 865.
- [19] J.G. Simmons, *J. Appl. Phys.* 34 (1963) 1793.
- [20] G. Wang, T.-W. Kim, Y.H. Jang, T. Lee, *J. Phys. Chem. C* 112 (2008) 13010.